Global map of solid Earth surface heat flow

J. Huw Davies

School of Earth and Ocean Sciences, Cardiff University, Main Building , Park Place, Cardiff CF10 3YE, UK

[1] A global map of surface heat flow is presented on a $2° \times 2°$ equal area grid. It is based on a global heat flow data set of over 38,000 measurements. The map consists of three components. First, in regions of young ocean crust (<67.7 Ma) the model estimate uses a half-space conduction model based on the age of the oceanic crust, since it is well known that raw data measurements are frequently influenced by significant hydrothermal circulation. Second, in other regions of data coverage the estimate is based on data measurements. At the map resolution, these two categories (young ocean, data covered) cover 65% of Earth's surface. Third, for all other regions the estimate is based on the assumption that there is a correlation between heat flow and geology. This assumption is assessed and the correlation is found to provide a minor improvement over assuming that heat flow would be represented by the global average. The map is made available digitally.

1. Introduction

[2] Earth's surface heat flux is a fundamental output of the dynamic solid Earth's heat engine. Therefore, a better understanding of Earth's surface heat flux provides a constraint on the internal state of the mantle, its evolution and geochemistry [*Davies*, 1989; *Dye*, 2012; *Korenaga*, 2008; *Loyd et al.*, 2007; *McDonough and Sun*, 1995; *Schubert et al.*, 1980; *The KamLAND Collaboration*, 2011]. It also provides a constraint on the thermal structure of the crust and lithospheric mantle [*Furlong et al.*, 1995], and hence to lithospheric rheology, which is sensitive to temperature [*Houseman et al.*, 1981; *Ranalli*, 1987]. The thermal structure of the near surface can also play a role in applica-

tions such as hydrocarbon exploration [*Tissot et al.*, 1987], geothermal exploration [*Muffler and Cataldi*, 1978], and mineral exploration [*Cathles and Smith*, 1983]. Earth's surface heat flux is also one of the ways that the solid interior couples to the hydrosphere, cryosphere, and atmosphere [*Fahnestock et al.*, 2001; *Mashayek et al.*, 2013; *Scott et al.*, 2001], while the thermal structure can also influence nonvolcanic release of volatiles such as CO_2 and methane from the crust [*Etiope and Klusman*, 2002; *Mörner and Etiope*, 2002].

[3] In terms of constraining mantle convection (and composition), a direct estimate of global heat flux is very useful. Such estimates continue to be refined and are agreeing at around 44–47 TW [*Davies and Davies*, 2010; *Jaupart et al.*, 2007;

Jessop et al., 1976; *Lee and Uyeda*, 1965; *Pollack et al.*, 1993; *Simmons and Horai*, 1968]. In contrast many of the processes mentioned above would benefit from an estimate of the spatial distribution of heat flux globally, e.g., for understanding controls of lithosphere rheology on deformation [*Bird et al.*, 2008; *Iaffaldano and Bunge*, 2009]. Unfortunately, global maps of surface heat flow are not as common as global estimates of total output. Equally regional maps [e.g., *Blackwell and Richards*, 2004] are more common than global maps. *Pollack et al.* [1993] presented a 5° × 5° global map, and also a map based on a spherical harmonic representation out to harmonic degree 12. *Bird et al.* [2008] produced a slight extension on the work of *Pollack et al.* [1993] for their application requiring global heat flow to constrain lithosphere rheology. *Goutorbe et al.* [2011] in their paper produce global maps of surface heat flow filtered with a Gaussian filter with a 500 km radius.

[4] I believe that it is now opportune to provide an attempt at a higher resolution map of Earth surface heat flow. This is partly motivated by the increasing magnitude of the heat-flow data set, improvements in digital geology maps and maps of ocean crustal age. It is also motivated by the increasing interest in the output as outlined earlier in section 1 (the author has been approached by at least one member of each of the above application domains for a digital global heat flow map). In addition, there are improved Geographical Information Systems (GIS) software tools that help analysis of such large digital data sets. I will next present an introduction to the data sets and methods used to develop a revised global map of surface heat flow.

2. Method

2.1. Overview of Method

[5] The global heat flux map consists of three major components. First, since young ocean crust data is affected by hydrothermal circulation [*Lister*, 1980] a model estimate is used in such regions rather than the raw data measurements. Second, in other regions of the world with measurements, those provide the estimate. Third, in all other regions the estimate is developed by assuming that there is a correlation between heat flow and geology, and the estimate is based on a weighted area

estimate of the heat flow. I will now briefly describe these component data sets.

2.2. Heat Flow Data

[6] The raw heat-flow data set, consisting of 38,374 heat flow values, used in *Davies and Davies* [2010], was provided by Gabi Laske and Guy Masters (http://igppweb.ucsd.edu/~gabi/rem.html). It was compiled from the literature and was an extension of the data set incorporated in the Global Heat Flow Database of the International Heat Flow Commission currently under the custodianship of William D. Gosnold (http://www.heatflow.und.edu/) which incorporates the work of many workers including for example *Gosnold and Panda* [2002], *Pollack et al.* [1993], *Jessop et al.* [1976], *Simmons and Horai* [1968], and *Lee and Uyeda* [1965]. Obvious data blunders were removed, including values around 0° latitude 0° longitude, and old heat flow values in the Barents and Kara Sea that conflict with more recent maps [*Tsybulya and Sokolova*, 2002].

[7] In Figure 1, I present the spatial distribution of the heat flow measurements. In regions of dense sampling, there are so many points that in the figure only a subset are visible. Even so, it is possible to see that there are some large-scale patterns to the values, and also that the spatial distribution of measurements is very inhomogeneous. The main issue in providing a global map of heat flow is how to cope with the regions with few or no measurements.

2.3. Equal Area 2° Grid

[8] It was decided to present the map on a 2° equal area grid. This decision followed an earlier investigation, not presented here, on a 1° equal area grid. This (1°) was deemed to be too high a resolution since less than 15% of the grid cells had heat flow measurements. At the 2° equal area, grid scale 40% of the grid cells have heat flow measurements (we note 15% are in young ocean crust, i.e., 15/40 ~37% of these grid cells). The grid of 10,312 cells is presented in Figure 2a and a zoomed in figure of the grid on Europe in Figure 2b. This illustrates that the area of an individual cell approximates the surface area, for example, of Switzerland. *Goutorbe et al.* [2011] show that the heat flow data set has large spatial variability even at very short length scales (<50 km). A 2° grid therefore cannot be expected to capture this variability but hopefully can capture some of the longer scale length
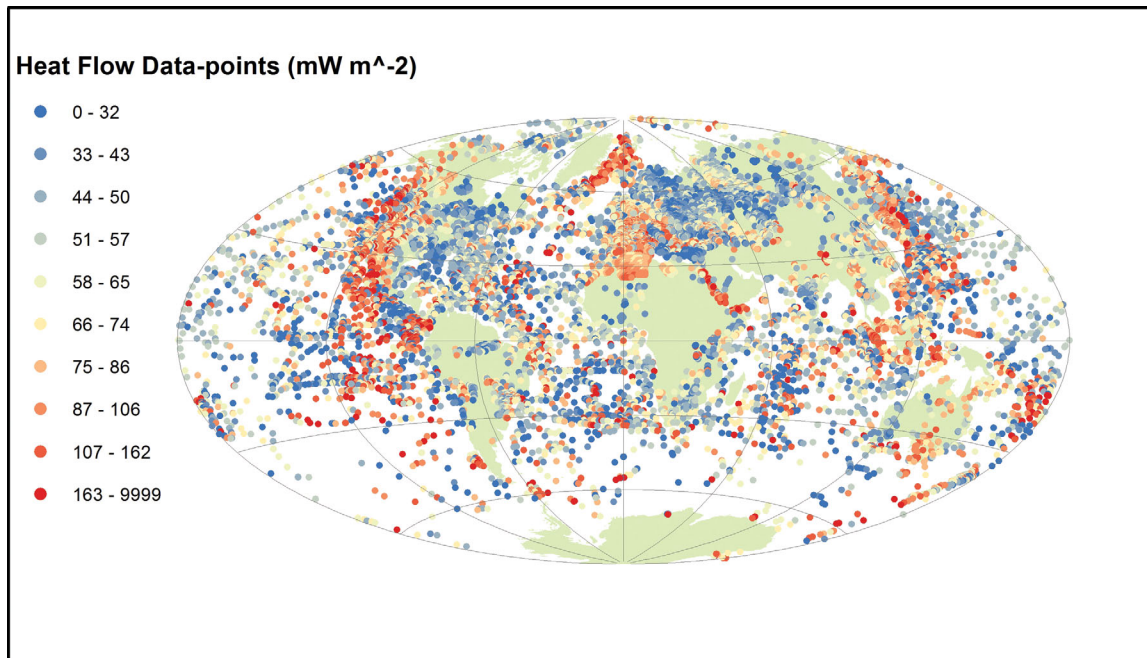
Figure 1. Map of heat flow measurement points. Many data points are hidden by later plotted points. Note the very inhomogeneous distribution (Aitoff World Projected Projection).

variability, which might be expected to reflect deeper processes.

2.4. Young Ocean Crust

[9] It has been argued that the very high scatter of heat flow values seen in young ocean basins primarily reflects the effect of hydrothermal circulation [*Hasterok*, 2013; *Lister*, 1980]. *Von Herzen et al.* [2005] argue that heat flow measurements in younger crust made in sedimented basement lows, for easier penetration of heat flow equipment, are biased downwards. They are biased downwards since while the up flow and hot regions tend to be basement highs and outcrops the basement lows in contrast have suffered diffuse down flow and had heat extracted by hydrothermal circulation [*Stein and Stein*, 1994]. As a result, it is argued that the average of the raw measurements is not representative of the heat flow [*Hasterok et al.*, 2011]. *Wei and Sandwell* [2006] estimate heat flow, using bathymetry as a function of age since the cooling and subsidence away from the ridge is a measure of the heat energy lost. Their results are also in excellent agreement with half-space cooling models, again suggesting that hydrothermal circulation is significant. These interpretations are further supported by the fact, known for a long time, that the ridges are not associated with a significant free-air gravity anomaly and therefore must be close to isostatic equilibrium [*Talwani et al.*, 1965]. The

detailed modeling of near ridge conduction [*Davies et al.*, 2008] shows that the limitation of the half-space model at the ridge (predicts infinite heat flow) does not affect heat flow estimates [*Davies and Davies*, 2010]. *Hasterok et al.* [2011] show that measurements taken in regions with thick, low permeability sediment cover are well fit by a simple inverse square root of age relationship which would be expected from a half-space model.

[10] Therefore to limit the effects of hydrothermal circulation, I have applied a simple half-space model (equation (1)) in regions of young ocean crust

$$Q = Ct^{-0.5} \qquad (1)$$

where Q is surface heat flow (mW m^{-2}), t is age (Myr), and C is a constant (mW m^{-2} Myr$^{0.5}$). I use the value $C = 490$ mW m^{-2} Myr$^{0.5}$, as derived by *Jaupart et al.* [2007]. They derive this value by using data beyond the age affected by hydrothermal circulation and adding the additional data point that conductive heat flow would be zero at infinite age.

[11] For the age of the oceanic crust, I use the model of *Seton et al.* [2012], a development from *Müller et al.* [1997] shown in Figure 3. It consists of 2,315,480 polygons. The half-space model is only applied out to 67.7 Ma which is a well-
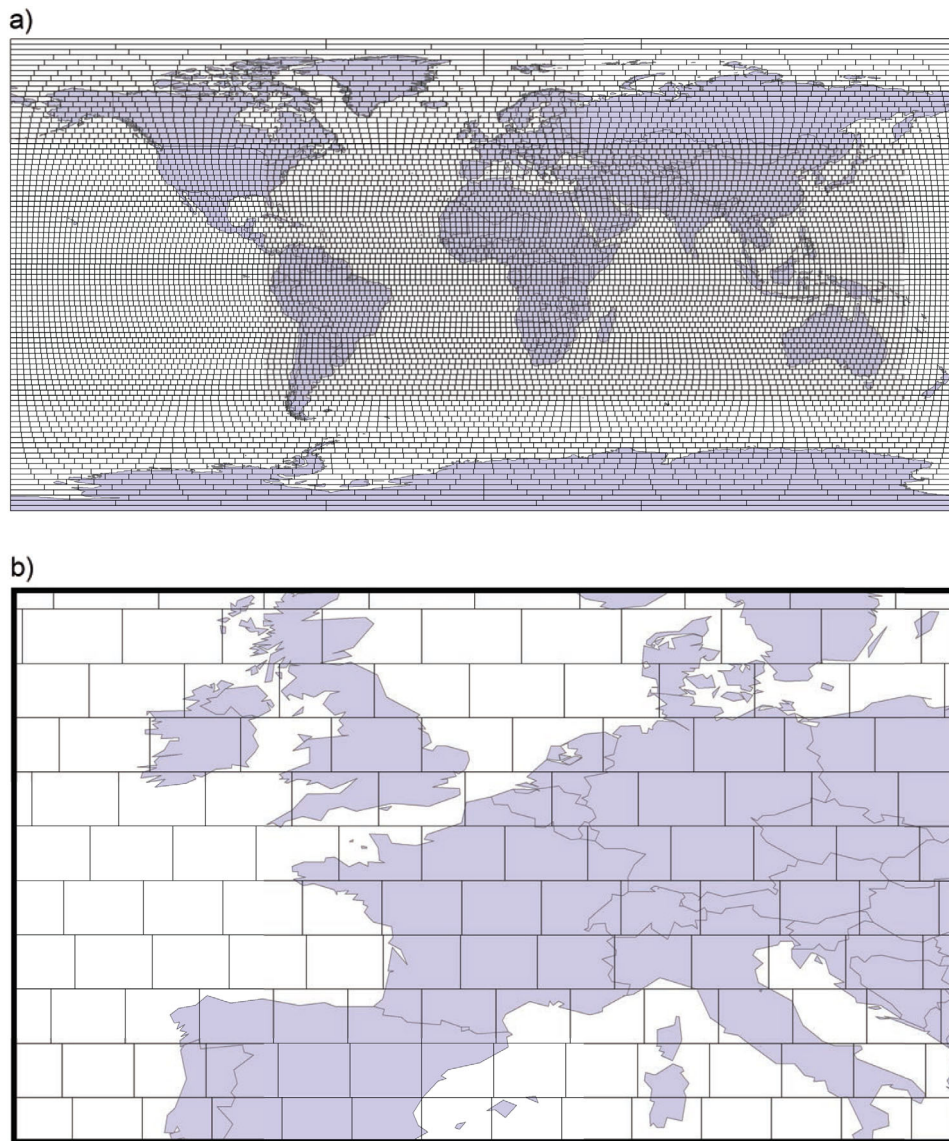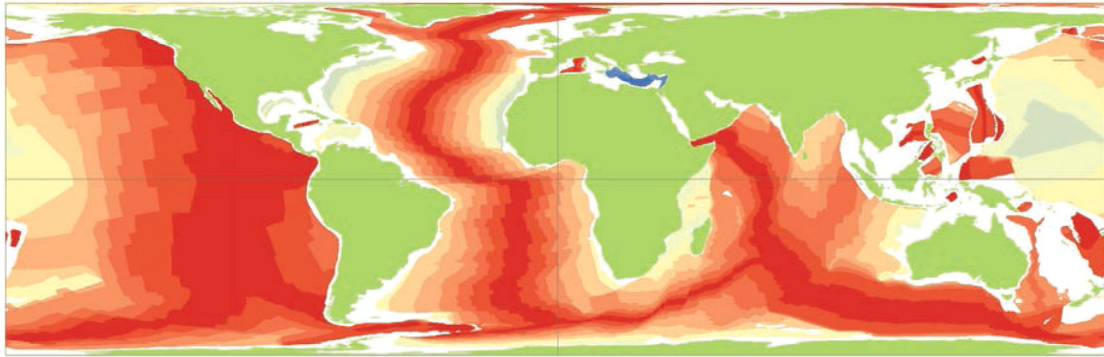
Figure 2. The 2° equal area grid. (a) The global map illustrates that the grid lines are equally spaced in latitude, but their spacing in longitude increases the further away one is from the equator. (b) A view of the grid overlying Western Europe. The map uses a Cylindrical Equal Area Projection. This projection is used for all following maps.

defined isochron in the *Seton et al.* [2012] model and around the age at which hydrothermal circulation is seen to play no role [*Stein and Stein*, 1997]. The resulting predicted heat flow, by applying equation (1) to the map of ocean age, is shown in Figure 4.

2.5. Description of Geology Data Set

[12] In grid cells that are not young oceanic crust and do not have measured heat flow values I predict the heat flow assuming that it is related to the observed geology following other studies [e.g.

Davies and Davies, 2010; *Pollack et al.*, 1993]. In this study, I use the digital geology data set CCGM/CGMW [*Commission for the Geological Map of the World*, 2000], abbreviated to CCGM (the French initials for the data set—Commission de la Carte Géologique du Monde). It covers the whole globe using 14,202 polygons. The CCGM has 51 geology units which are defined by Lithology and Stratigraphy. *Davies and Davies* [2010] used CCGM in combination with a second geology data set, the Global GIS data set [*Hearn et al.*, 2003]. Later, I will test the value of the assumption that heat flow might be related to geology. As a

Age Ocean Crust (Ma)

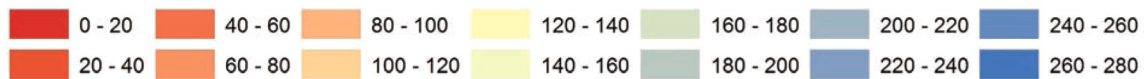|							
0 - 20	40 - 60	80 - 100	120 - 140	160 - 180	200 - 220	240 - 260
20 - 40	60 - 80	100 - 120	140 - 160	180 - 200	220 - 240	260 - 280

Figure 3. Map of the age of the ocean crust in millions of years before present (Ma) from *Seton et al.* [2012].
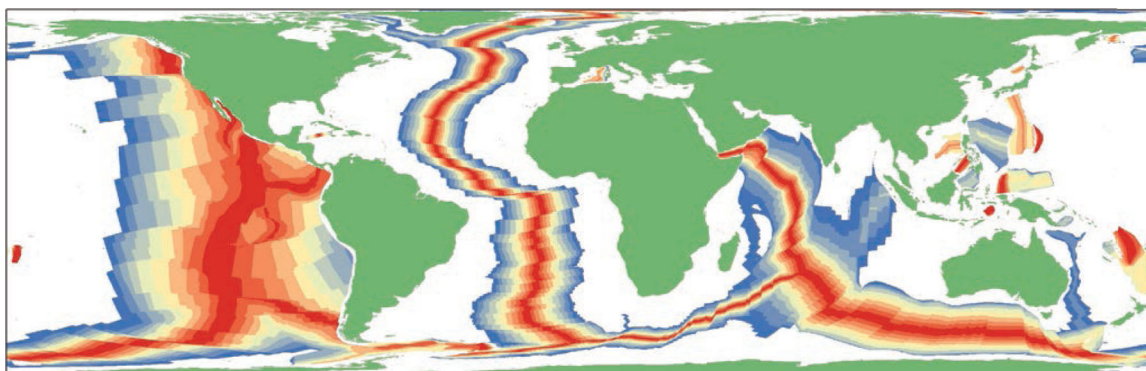
result of such tests undertaken at a 1° equal area scale (not presented here), it was discovered that using the CCGM geology alone, gave a slightly better prediction than using it in combination with the Global GIS data set. Therefore, in this work only the CCGM geology is used.

2.6. GIS Methods

[13] The heat flow was calculated on the 2° equal area grid in the following steps:

[14] 1. The 2° grid was unioned with the CCGM geology data set (i.e., the geology polygons were cut by the grid to limit the geology polygons to be contained by the 2° grid, e.g., *Davies and Davies* [2010]). The area of each resulting unioned polygon was evaluated.

[15] 2. The heat flow points were spatially joined (i.e., the heat flow value was assigned to the polygon that contained the point) with the unioned polygons from step 1. For polygons containing more

Young Ocean Crust Heat Flow (mW m^-2)

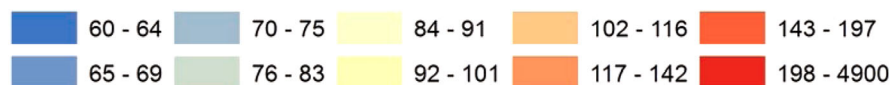|				
60 - 64	70 - 75	84 - 91	102 - 116	143 - 197
65 - 69	76 - 83	92 - 101	117 - 142	198 - 4900

Figure 4. Map of the predicted heat flow in regions with oceanic crust younger than 67.7 Ma. Prediction uses equation (1) and the ages from Figure 3, area weighted. The legend uses deciles for the classes. The same legend classification is used for all the following maps unless otherwise stated.

than one heat flow point, the average heat flow was assigned to each polygon.

[16] 3. For each unioned polygon with a heat flow value, the product of the average heat flow and area was evaluated.

[17] 4. A summarize operation was run for the grid cells, over the polygons with heat flow values, to obtain the (i) sum of the area of unioned polygons and the (ii) sum of the product of area and heat flow for the unioned polygons. What this means is that for all unioned polygons with a heat flow value, that fall within a grid cell, the sum of their areas was evaluated and recorded in a new field; and also the sum of the product of their area times heat flow in another field.

[18] 5. For each grid cell (with observations), the sum of the product of the area and heat flow was divided by the sum of the area for polygons with heat flow values (both produced by step 4). This gives the area weighted heat flow estimate from the data for each grid cell with data. The result is presented in Figure 5a. Figure 5b shows the number of heat flow measurements contributing to each cell estimate.

[19] 6. The young oceanic crust age polygons were also spatially joined to the 2° equal area grid, and an area-weighted heat flow was assigned to each 2° cell (using a GIS field calculation), i.e., a 2° grid version of the result already presented in Figure 4.

[20] 7. The results of steps 5 and 6 were combined such that grid cells used the data-based estimate only in areas outside young oceanic crust.

[21] 8. The heat flow data points spatially joined to the unioned geology/grid polygons, from step 2, were also used to derive an area-weighted estimate of the average heat flow for each geology (i.e., summarize operation was done on the geology class, similar to steps 2–5). Figure 6 symbolizes the result on the original unioned polygons.

[22] 9. Cells with no values after step 7 were assigned the area-weighted (areas derived after step 5) average heat flow derived for each geology in step 8.

[23] 10. The final result, an estimate of heat flow in each 2° equal area grid cell, is the combination of steps 7 and 9 (Figure 7).

[24] The above method calculates the area-weighted mean. In addition, the result was calculated assuming the median of the data measurements and the median of the geology correlation in the unioned polygons; and then also the median of the heat flow value in the union polygons in a grid cell. The method in this case is slightly different in that the union of the grid and geology is joined to the heat flow measurements and not the reverse, and the medians are evaluated outside the GIS software using a bespoke "C" code. The final result again used a weighted average. This result is presented in Figure 8. A simplified flow diagram of the methods is presented in Figure 9.

[25] The variance of the data estimate was calculated, including a sample-sized unbiased estimate [*Rimoldini*, 2013]. The square root of this variance was used as an estimate of the error of the heat flow estimate for 2° polygons which had more than one contributing polygon. The error for the young ocean crust was estimated following *Davies and Davies* [2010] who assumed an error of 30 mW m^{-2} for C in equation (1). This is slightly increased from the 20 mW m^{-2} suggested by *Jaupart et al.* [2007]. The increase accounts for the uncertainty also in the area of different age ocean floor. For all other 2° polygons, a straightforward error estimate was undertaken assuming that it was some 10% less than the standard deviation of the heat flow data in the 2° grid cells with heat flow data. This gave an error estimate of 41.5 mW m^{-2}.

2.7. Antarctica

[26] Using the data and geology-based estimate for Antarctica would lead to a constant and high value across the whole continent. This is because the very few measurements in the data set are from West Antarctica alone. It is likely that the larger part of the continent, East Antarctica, does not have such high values. I have therefore improved the map in Antarctica following both *Shapiro and Ritzwoller* [2004] (who used shear wave velocities in the upper mantle as a proxy of heat flow) and *Maule et al.* [2005] (who used the strength of the magnetic field as a heat flow proxy). So, for Antarctica, led by the similar estimates of *Shapiro and Ritzwoller* [2004] and *Maule et al.* [2005] and the limited measurements I set the values for East Antarctica (from ∼50°W to 180°E) to 65 mW m^{-2} and in West Antarctica (from ∼50°W to 180°W) to 100 mW m^{-2}.

2.8. Coverage

[27] The young ocean crust category covers around 40% of the final map, while cells obtaining

a)

Area-weighted Data based Heat Flow estimate on 2 degree grid (mW m^-2)

no data	33 - 41	48 - 53	59 - 64	73 - 84	108 - 1237
1 - 32	42 - 47	54 - 58	65 - 72	85 - 107	

b)

Number of Heat Flow measurements per cell

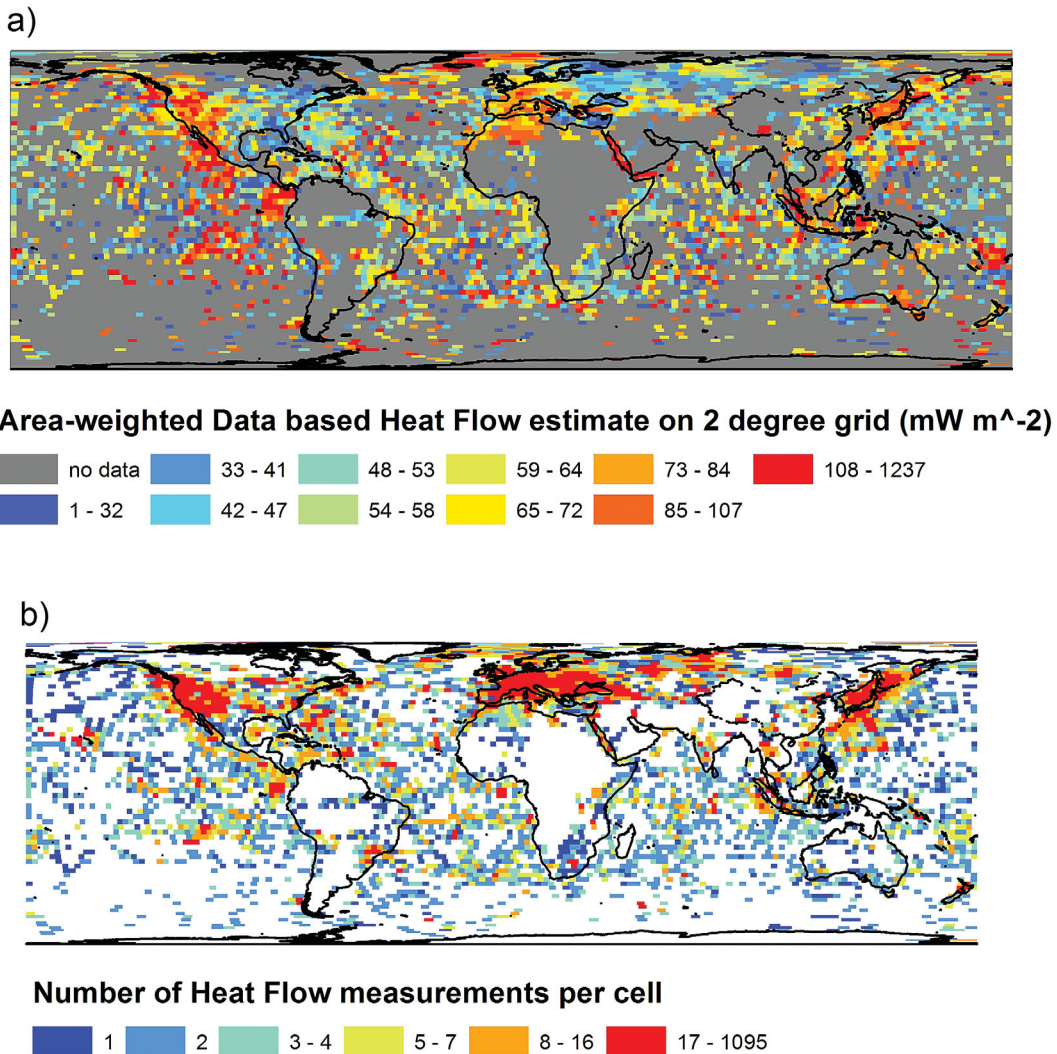| 1	2	3 - 4	5 - 7	8 - 16	17 - 1095

Figure 5. (a) Area weighted heat flow on the 2° equal area grid in regions with heat flow measurements and (b) global map of the number of heat flow measurements in each cell.

their value from the raw data cover around 25% of the final map (though as mentioned earlier this would be 40% if I included data in the young ocean crust regions). This leaves around 35% of the cells uncovered by either previous category and their value is obtained assuming a correlation with the underlying geology. Further details of the coverage are presented in Figure 5b which shows the number of heat flow measurements contributing to each cell estimate. We see that the peak is 1095, but many cells have fewer than five measurements.

3. Results

[28] The final map using the mean is presented in Figure 7, while the preferred final map based on the median is presented in Figure 8. Note

neither map is smoothed. As a result, the maps are somewhat speckled reflecting the large spatial variability of the underlying data. The spatial variability of density of actual heat flow values was illustrated in Figure 5b. In spite of this large spatial variability, the map demonstrates large coherent variation in many regions. This is of course true in the young oceans due to the assumption of correlation with age, which is spatially smoothly varying. Equally regions with no measurements and relatively homogeneous geology will also have relatively homogeneous heat flow predictions.

[29] The obvious trends in the maps are the high heat flow over young ocean crust including active back arc basins and the low heat flow over continental shields and cratons. While it is not useful
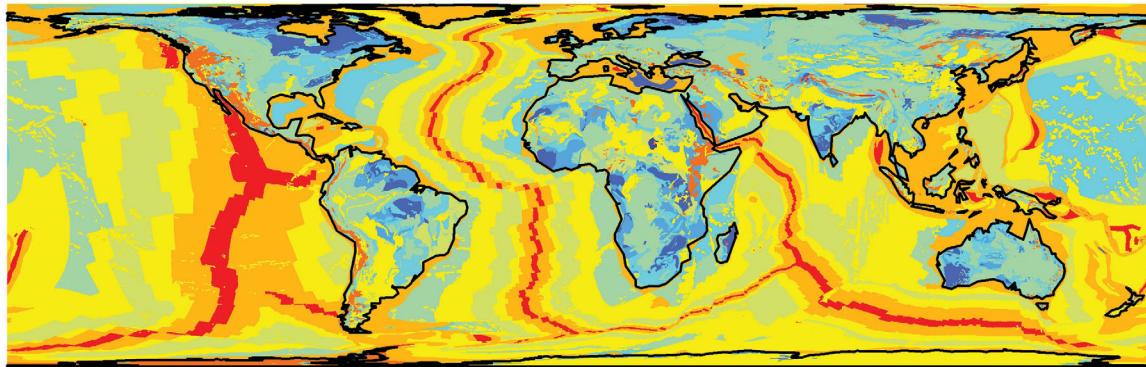
Heat Flow based on Geology (mW m^-2)

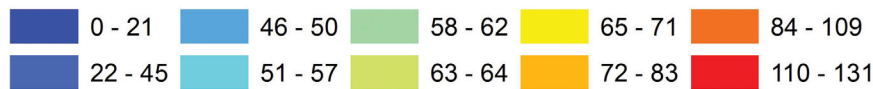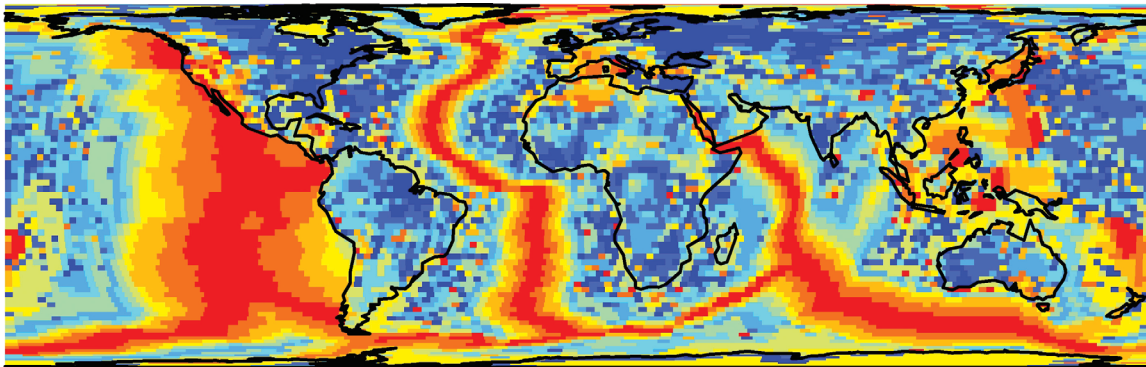|				
0 - 21	46 - 50	58 - 62	65 - 71	84 - 109
22 - 45	51 - 57	63 - 64	72 - 83	110 - 131

Figure 6. Global map showing the heat flow assuming that a correlation between heat flow and geology held everywhere.

for the reader to be presented with all regions in detail, I focus on two regions to illustrate the character of the map.

[30] First, I focus in on Western Europe (Figure 10). We observe high heat flow is present in Iceland and the mid-Atlantic ridge as might be expected. Also there is low heat flow in Scandinavia and Russia as might be expected given the old stable lithosphere. We note that regions of high heat flow are mapped in central France, parts of Italy, the Western Mediterranean, Pannonian basin, northern Greece, northern Turkey, the Red Sea, and Algeria. Low heat flow is mapped in the Adriatic, the Eastern Mediterranean (excluding the Aegean), and eastern Atlantic. Such distributions are not unreasonable given our understanding of the tectonics of Europe. If they are accurate then it is probably a result of the high data density.

[31] Second, I focus on central North America (Figure 11). This figure shows high heat flow

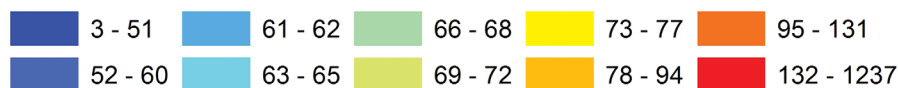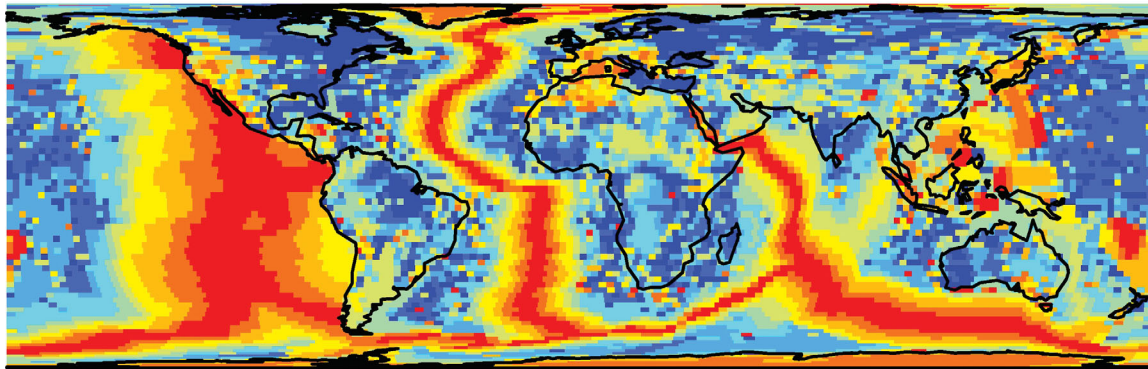## Final Estimate of Heat Flow (mW m^-2) (Area-weighted Mean)

3 - 51	61 - 62	66 - 68	73 - 77	95 - 131
52 - 60	63 - 65	69 - 72	78 - 94	132 - 1237

Figure 7. Global map of Earth Surface Heat Flow, in mW m^{-2}. It uses the individual components given by Figures 4–6. All component estimates were derived using the mean.

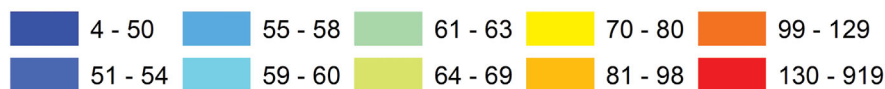**Final Estimate of Heat Flow (mW m^-2) (Area-weighted Median)**

4 - 50	55 - 58	61 - 63	70 - 80	99 - 129
51 - 54	59 - 60	64 - 69	81 - 98	130 - 919

Figure 8. Global map of Earth Surface Heat Flow, in mW m^{-2}. It uses the ocean heat flux estimate given by Figure 4, but the data and geology correlation components use the median as opposed to the mean in deriving the estimate in the unioned polygons.

around the ridges in the Pacific, also in regions of the west of the USA (Yellowstone, Basin and Range, Rio Grande), parts of the Caribbean and a few single grid cells in the Atlantic (e.g., Bermuda). Low heat flow is mapped in the east of North America, especially cratonic Canada, parts of the Gulf of Mexico and southeastern USA. Again, the predictions are probably good in regions of high data coverage.

[32] While the target of this work, in contrast to *Davies and Davies* [2010], was not to produce an estimate of the global surface heat flux, I note that the map in Figure 7 would predict an average heat flow of around 86 mW m^{-2} (83 mW m^{-2} using the median estimator), giving a total estimate of Earth surface heat flux from the interior of ~44 TW. While limitations in the result are discussed in section 4, it is worth noting here that this estimate is uncertain especially due to uncertainties in the young ocean crust heat flow. Using the logic of *Davies and Davies* [2010] and *Jaupart et al.* [2007], a further 1 TW should be added to account for the heat flow resulting from plumes which are unaccounted for by the half-space model in the young ocean crust (since the parameter C in equation (1) for the half-space model is derived by excluding regions of the oceans believed to be affected by plumes), which would lead to a final value of ~45 TW. It is interesting to note that the mean continental heat flow (including arcs and continental margins) is 64.7 mW m^{-2}, while the mean oceanic heat flow is 95.9 mW m^{-2}.

4. Discussion

[33] I suggest that certain aspects of Earth surface heat flux are quite well captured by the map. For example, the low heat flow of continental shields and cratons and the high heat flow of young ocean crust. There are other regions though where one might question the map. For example might we expect the heat flow to be higher in general in the East African Rift than shown on the map? We note there are a few grid cells with high values. This limited number of grid cells with high heat flow value is possibly because there are very few actual measurements in the East African Rift and the prediction therefore is dependent on the correlation with geology. Below I discuss this correlation between geology and heat flow and show that it has value. The value though is shown to be moderate only, so one should not expect it to always be successful.

4.1. Scale

[34] A fundamental decision in this process was the choice of the grid scale. It was decided to go for as fine a scale as possible but not so fine that the geology correlation component part of the map was too significant. It was decided that at 1° scale the map would have too little coverage from the data. At 2° scale, the geology correlation component was reduced to 35% and such a map could provide reasonable resolution in regions of good coverage. I note that *Pollack et al.* [1993] at 5° ×

Evaluate heat flow in cells with ocean crust younger than 67.7Ma using age and half-space model (eq 1)

Evaluate value in remaining cells with Heat Flow Data using the mean (fig7) or median (fig 8) value area-weighted

Evaluate value in remaining cells using area-weighted mean assuming correlation between geology and heat flow using mean (fig 7) or median (fig 8)
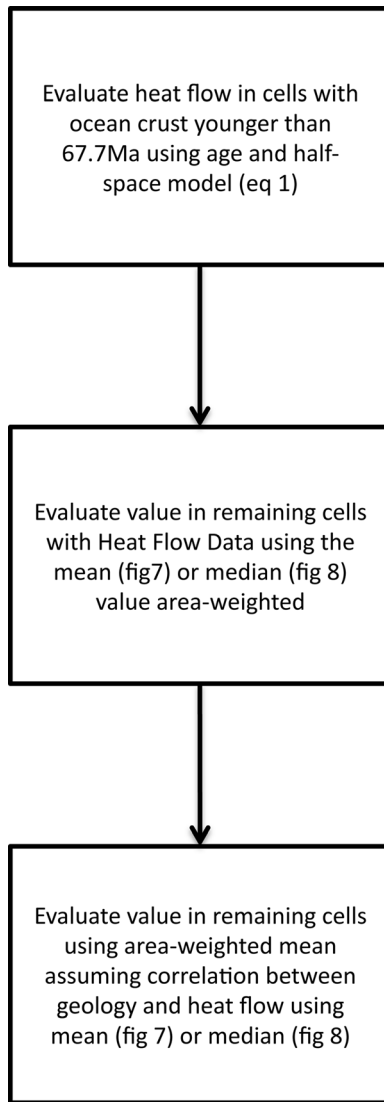
Figure 9.   Simplified flow diagram of the workflow.

5° (2592 cells) had a 65% global coverage from data.

4.2.   Correlation Between Geology and Heat Flow

[35]   A large proportion of the map (35%) is based on an assumed correlation between heat flow and geology. I have made a test of this assumption in regions with actual measurements. I have done this by comparing the prediction from the geology with the actual data estimate. Figure 12 presents a map of this anomaly.

[36]   I have evaluated a second anomaly by comparing the observational estimate in these cells with the global average heat flow. I find that the

geology-based estimate is better and reduces the range between the 1st and 3rd quartile by 10% more than using an estimate based on a straight average of relevant heat flow measurements. Therefore, while I demonstrate that the geology correlation has value, the value is limited. We note that while this comparison is useful it is not a proper bootstrap comparison which is impractical given the workflow.

4.3.   Limitations

[37]   This study has many further limitations, with the most important ones all reflecting the difficulty of making high-quality heat flow measurements. Critically, the number of observations is limited and spatially very inhomogeneous. Even in regions with measurements the data quality varies. Many of the original data have estimates of the quality, but this is not present for all measurements. I have here taken the decision to use virtually all the data to have a broader spatial coverage hoping that statistical averaging will limit the pollution of the result by poor measurements. In other cases, the raw measurements might be good but the scientists might not have corrected for local processes that could be affecting them as estimates of the deep heat flow (e.g., topography [*Jeffreys*, 1938], palaeoclimate effects [*Jessop*, 1971; *Rolandone et al.*, 2003; *Sass et al.*, 1971], advection by fluids [*Beardsmore and Cull*, 2001], erosion and sedimentation [*Benfield*, 1949]). In cells with multiple measurements, the spread in values in each cell is usually very high, as found by *Goutorbe et al.* [2011] and *Davies and Davies* [2010]; therefore, the error in the mean can be quite high especially for cells with only a few measurements. These limitations could explain why some individual pixels seem to predict values that are probably unreasonable as estimates of the broader heat flow over a 2° grid cell. For example, some continental pixels have values above 120 mW m^{-2} and such values in continental areas would suggest extensive melting which is not common in the crust [*Chapman*, 1986]. In some cases, these values might reflect more localized heat flow while in other cases they might reflect other processes as described above that have not been corrected for.

[38]   In addition to statistical variation, the map could also suffer from possible bias. For example, one might speculate that the raw data set might have a spatial bias resulting from scientists being preferentially attracted to areas of extreme heat flow, especially high heat flow values, also driven by potential geothermal applications. This
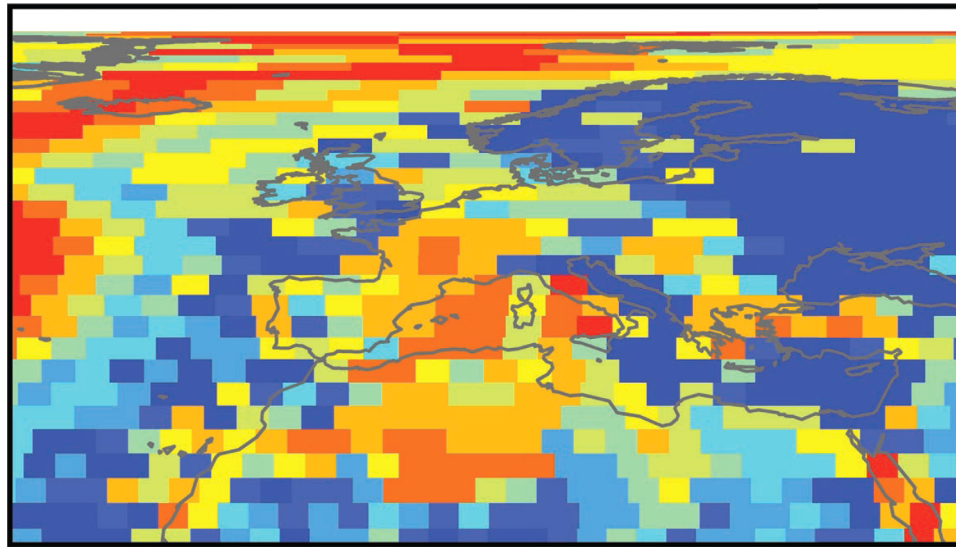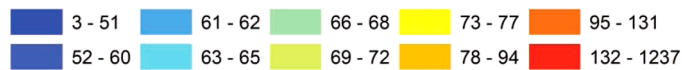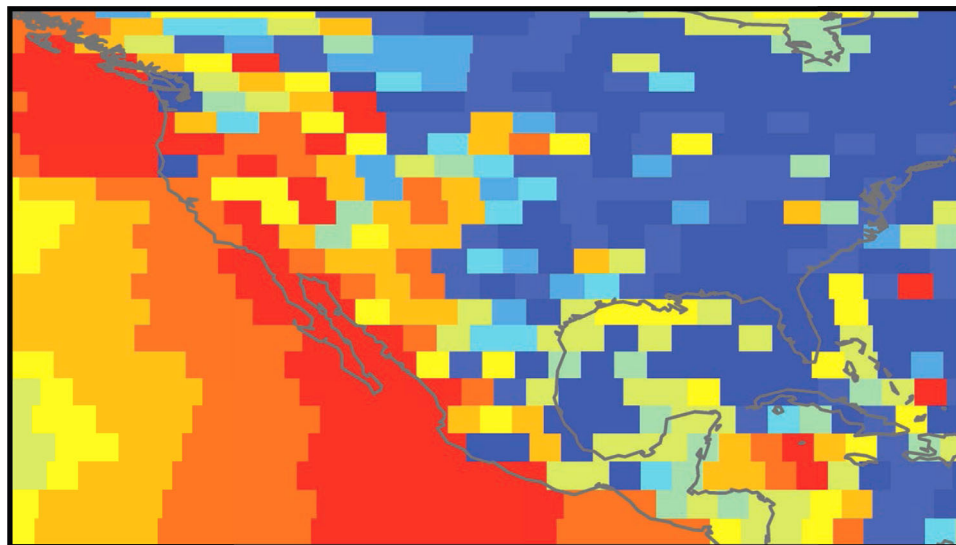
Figure 10. The estimated surface heat flux beneath Europe and surroundings; i.e., a zoomed in version of Figure 7.

speculation can only be confirmed/denied by further measurements. The use of area-weighted estimates in our methodology is an attempt at reducing this problem.

[39] The estimate for the heat flow in a cell based on measurements using a straight arithmetic average could suffer from the effect of outliers. Since the distribution of heat flow measurements is
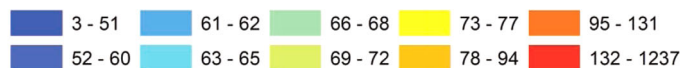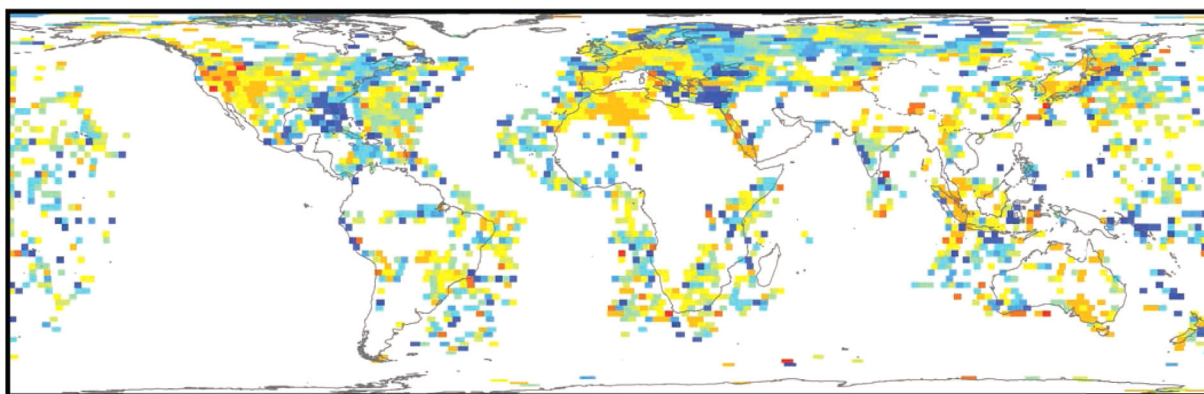

Figure 11. The estimated surface heat flux beneath central North America; i.e., a zoomed in version of Figure 7.

Figure 12. Global map of the difference between the heat flow estimate in a cell based on data and the geology correlation (where both exist—excluding young ocean crust). Classification is based on Natural Breaks (Jenks).

skewed toward high values, the derived values could possibly be biased higher. This could also be the case when deriving the relationship between heat flow and geology. A possibly more robust alternative would be to use the median of the values rather than the mean. As mentioned, this has been undertaken and the results are presented in Figure 8. One can see that while Figures 7 and 8 are broadly the same the "speckles" do not always correspond. One might imagine that these "unstable" pixels might be less robust. There was no significant difference in the standard deviation of the mean and median estimate of the heat flow. Using the area-weighted estimate possibly further moderates the effect of outliers where present.

[40] The estimate of heat flow in young ocean crust depends upon the half-space formulation. While I argue that the estimate presented is the best possible given the current understanding, the models hopefully can be improved in the near future. Aspects that could benefit from further consideration are the variation in ocean crust material properties with temperature and pressure [*Afonso et al.*, 2005; *Grose*, 2012; *McKenzie et al.*, 2005], the variation from one ocean basin to another [*Marty and Cazenave*, 1989], and improved understanding of hydrothermal circulation [*Schmeling and Marquart*, 2013; *Theissen-Krah et al.*, 2011]. Also with more data the estimation of the parameter values required by these models can be improved.

[41] As already mentioned, the use of geology to predict heat flow in regions with no actual heat flow measurements has value, but as described this is limited. This is a similar conclusion to *Jaupart and Mareschal* [2011] who suggest that there is only a weak relationship such that geology is not a good proxy. *Goutorbe et al.* [2011] investigate using multiple proxies for estimating heat flow. Using such methods it might be possible to make better estimates in regions with no data if more proxy data sets were used. Proxies that have been used successfully by others to estimate heat flow include shear wave velocities in the upper mantle [*Shapiro and Ritzwoller*, 2004] and the strength of the magnetic field [*Maule et al.*, 2005].

[42] Ultimately though, nothing will help overcome these limitations more than getting additional high quality, well corrected, heat flow measurements. This is especially true both in regions with few measurements only and in regions where current estimates might be affected by processes unaccounted for. For example, limited measurements might be affecting the high value for Minnesota (Figure 11), while water flow might lead to the low values in the Adriatic (Figure 10). There are now of course many workers who are correcting heat flow measurements, a notable example for Europe being *Majorwicz and Wybraniec* [2011]. The spatial coverage of the current work has already been described in section 3. Figures 1 and 5 illustrate regions most in need of

additional measurements. These include the polar regions, much of the oceans, especially the southern oceans, Africa, parts of Asia, Canada, and South America. Until there are many more measurements, work such as this through the steps outlined above, try to limit these issues where possible and provides a "map" of Earth surface heat flux.

5. Data Sets of the Map

[43] This map/model is made available (associated with this publication) in two formats on two grids. This is Data_Table1 (see supporting information).[1] The first grid is the actual grid on which it is produced—i.e., the heat flow value of the grid cell is assigned to the centroid of each 2° equal area cell (i.e., with 10,312 values, and label Eq_area in file name). The second grid is a regular 2° latitude × 2° longitude grid (i.e., 16,200 values, and label Eq_Lon_Lat in file name). Again the heat flow value assigned to each point is the value of the grid cell that contains it. Both data sets are provided in an ASCII text format in five columns, which are longitude, latitude, heat flow mean value, heat flow median value, and error. These two files are each provided in two forms, a tab delimited (_tab.txt file ending) and a comma delimited format (.csv file ending). The longitude and latitude are in decimal degrees, with west and south being negative longitude and latitude, respectively; while heat flow is in mW m^{-2}.

[45] The data on the equal area grid is also provided as a polygon shapefile, called *Heat_Flow*. It uses a geographic coordinate system and the North American 1927 datum. The attribute table contain fields recording (i) the Final Heat Flow estimate [Final_HF_mean] (based on young crust estimate, where present; otherwise uses the mean estimate based on raw data; and if no raw data uses a mean estimate based on the correlation with geology), (ii) the Final Heat Flow estimate [Final_HF_median] based on the median, (iii) the estimate for Young Ocean Crust Heat Flow [Yng_OC_HF], where it exists—it is given a value of zero otherwise, (iv) [DataHFMeanArWghtd] is the estimate for the Heat Flow using the mean from the data in an area-weighted manner as described (note cells with no data record 0 in this file), (v) [DataHF_Median] is the estimate for the Heat Flow

using the median from the data in an area-weighted manner (note cells with no data record 0 in this file), (vi) the estimated heat flow based on the Geology using the mean [GeolMeanHF], (vii) the estimated heat flow based on the Geology using the median in an area-weighted manner [GeolMedianHF_median_Area_ weighted], (viii) error estimate [Total_Error], and (ix) the Longitude and Latitude for the centroid of the grid cell in degrees [Longitude] and [Latitude]. All heat flow values are in mW m^{-2}.

[46] Files for the separate components on the equal area grid are also provided. These are (i) Data_Table2_eq_area.csv, this is a csv file presenting the data-based estimate of heat flow using the median (in this file cells with no value are given the value −999.999), (ii) Data_Table3_eq_area.csv is a csv file with the heat flow based on age of ocean crust (in this file cells with no value are given the value −999.999), and (iii) Data_Table4_eq_area.csv is a csv file with the estimate based on the inference from geology, again cells with no values are given the value −999.999. The format of these files is three columns, longitude, latitude, and value. In (iv) Data_Table4_Eq_area.csv a longer version of the data file is presented with eight columns, longitude, latitude, number of contributing union polygons to heat flow estimate, number of raw contributing heat flow values, minimum value from raw heat flow values (not contributing polygons), maximum value of raw heat flow values in this polygon (not the maximum from the average of the contributing union polygons), median estimate of heat flow, area-weighted mean estimate of heat flow and square root of unbiased variance estimate (standard deviation) (cells with only one contributing do not have a variance defined and the cells have a value of −999.999). A final file (v) DataTable6_2deg_equal_area_grid_description.txt is presented detailing the grid. It has six columns, which are the longitude of the cell centroid, the latitude of the cell centroid, the west longitude of the cell, the east longitude of the cell, the southern latitude of the cell, and the northern latitude of the cell. This full set of files provides readers with sufficient information to make their own choices. In the author's opinion, the default map would be the map based on the median estimate of heat flow, as shown in Figure 8.

6. Summary

[47] This work presents the derivation of a global map of surface heat flux on a 2° equal area grid. It

---

uses a model for the conductive flow in regions of young ocean crust. In other regions, it uses the average of heat flow measurements where they are available. Finally, in all other grid cells, the estimate is based on the area-weighted average estimate based on the grid cell geology, assuming that there is a correlation between heat flow and geology globally. To facilitate usage of this map it is made available digitally in many formats.

Acknowledgments

References

Afonso, J. A., G. Ranalli, and M. Fernàndez (2005), Thermal expansivity and elastic properties of the lithospheric mantle: Results from mineral physics of composites, *Phys. Earth Planet. Inter.*, *149*, 279–306.

Beardsmore, G. R., and J. P. Cull (2001), *Crustal Heat Flow*, Cambridge Univ. Press, Cambridge.

Benfield, A. E. (1949), The effect of uplift and denudation on underground temperatures, *J. Appl. Phys.*, *20*, 66–70.

Bird, P., Z. Liu, and W. K. Rucker (2008), Stresses that drive the plates from below: Definitions, computational path, model optimization, and error analysis, *J. Geophys. Res.*, *113*, B11406, doi:10.11029/12007JB005460.

Blackwell, D., and M. Richards (2004), *Geothermal Map of North America*, Am. Assoc. of Pet. Geol., Tulsa, Okla.

Cathles, L. M., and A. T. Smith (1983), Thermal constraints on the formation of Mississippi Valley-type lead-zinc deposits and their implications for episodic basin dewatering and deposit genesis, *Econ. Geol.*, *78*, 983–1002.

Chapman, D. S. (1986), Thermal gradients in the continental crust, *Geol. Soc. Spec. Publ.*, *24*, 63–70.

Commission for the Geological Map of the World (2000), *Geological Map of the World at 1:25000000*, UNESCO/CCGM, Paris.

Davies, D. R., J. H. Davies, O. Hassan, K. Morgan, and P. Nithiarasu (2008), Adaptive finite element methods in geodynamics Convection dominated mid-ocean ridge and subduction zone simulations, *Int. J. Numer. Methods Heat Fluid Flow*, *18*, 1015–1035.

Davies, G. F. (1989), Mantle convection model with a dynamic plate: Topography, heat flow and gravity anomalies, *Geophys. J. Int.*, *98*, 461–464.

Davies, J. H., and D. R. Davies (2010), Earth's surface heat flux, *Solid Earth*, *1*, 5–24.

Dye, S. T. (2012), Geoneutrinos and the radioactive power of the Earth, *Rev. Geophys.*, *50*, RG3007, doi:10.1029/2012RG000400.

Etiope, G., and R. W. Klusman (2002), Geologic emissions of methane to the atmosphere, *Chemosphere*, *49*, 777–789.

Fahnestock, H., W. Abdalati, I. Joughin, J. Brozena, and P. Gogineni (2001), High geothermal heat flow, basal melt, and the origin of rapid ice flow in central Greenland, *Science*, *294*, 2338–2342.

Furlong, K. P., W. Spakman, and R. Wortel (1995), Thermal structure of the continental lithosphere—Constraints from seismic tomography, *Tectonophysics*, *224*, 107–117.

Gosnold, W. D., and B. Panda (2002), *The Global Heat Flow Database of The International Heat Flow Commission*. [Available at http://www.und.edu/org/ihfc/index2.html.].

Goutorbe, B., J. Poort, F. Lucazeau, and S. Raillard (2011), Global heat flow trends resolved from multiple geological and geophysical proxies, *Geophys. J. Int.*, *187*, 1405–1419.

Grose, C. J. (2012), Properties of oceanic lithosphere: Revised plate cooling model predictions, *Earth Planet. Sci. Lett.*, *333–334*, 250–264.

Hasterok, D. (2013), A heat flow based cooling model for tectonic plates, *Earth Planet. Sci. Lett.*, *361*, 34–43.

Hasterok, D., D. S. Chapman, and E. E. Davis (2011), Oceanic heat flow: Implications for global heat loss, *Earth Planet. Sci. Lett.*, *311*, 386–395.

Hearn, P. J., T. Hare, P. Schruben, D. Sherrill, C. LaMar, and P. Tsushima (2003), *Global GIS—Global Coverage DVD (USGS)*, Am. Geol. Inst., Alexandria, Va.

Houseman, G. A., D. P. McKenzie, and P. Molnar (1981), Convective instability of a thickened boundary layer and its relevance for the thermal evolution of continental convergent belts, *J. Geophys. Res.*, *86*, 6115–6132.

Iaffaldano, G., and H.-P. Bunge (2009), Relating rapid plate-motion variations to plate-boundary forces in global coupled models of the mantle/lithosphere system: Effects of topography and friction, *Tectonophysics*, *474*, 393–404.

Jaupart, C., and J.-C. Mareschal (2011), *Heat Generation and Transport in the Earth*, 464 pp., Cambridge Univ. Press, Cambridge.

Jaupart, C., S. Labrosse, and J.-C. Mareschal (2007), Temperatures, heat and energy in the mantle of the Earth, in *Treatise on Geophysics, v. 7 Mantle Convection*, edited by D. Bercovici, pp. 253–303, Elsevier, Amsterdam.

Jeffreys, H. (1938), The disturbance of the temperature gradient in the Earth's crust by inequalities of height, *Mon. Not. R. Astron. Soc.*, *4*, 309–312.

Jessop, A. M. (1971), The distribution of glacial perturbation of heat flow in Canada, *Can. J. Earth Sci.*, *8*, 162–166.

Jessop, A. M., M. A. Hobart, and J. G. Sclater (1976), *The World Heat Flow Data Collection, 1975*, 125 pp., Earth Phys. Branch; Energ. Mines and Resour. Canada, Ottawa, Ont.

Korenaga, J. (2008), Urey ratio and the structure and evolution of Earth's mantle, *Rev. Geophys.*, *46*, RG2007, doi:10.1029/2007RG000241.

Lee, W. H. K., and S. Uyeda (1965), Review of heat flow data, in *Terrestrial Heat Flow*, edited by W. H. K. Lee, pp. 87–190, A. G. U., Washington, D. C.

Lister, C. R. B. (1980), Heat flow and hydrothermal circulation, *Ann. Rev. Earth Planet. Sci.*, *8*, 95–117.

Loyd, S. J., T. W. Becker, C. P. Conrad, C. Lithgow-Bertelloni, and F. A. Corsetti (2007), Time variability in Cenozoic reconstructions of mantle heat flow: Plate tectonic cycles

and implications for Earth's thermal evolution, *Proc. Natl. Acad. Sci. U. S. A.*, *104*, 14,266–14,271.

Majorowicz, J., and S. Wybraniec (2011), New terrestrial heat flow map of Europe after regional paleoclimatic correction application, *Int. J. Earth Sci.*, *100*, 881–887.

Marty, J. C., and A. Cazenave (1989), Regional variations in subsidence rate of oceanic plates: A global analysis, *Earth Planet. Sci. Lett.*, *94*, 301–315.

Mashayek, A., R. Ferrari, and W. R. Peltier (2013), Geothermal heat flux and enhanced abyssal mixing: Implications for the Antarctic bottom water circulation, *Geophys. Res. Abstr.*, *15*, EGU2013–6310.

Maule, C. F., M. E. Purucker, N. Olsen, and K. Mosegaard (2005), Heat flux anomalies in Antarctica revealed by satellite magnetic data, *Science*, *309*, 464–467.

McDonough, W., and S. Sun (1995), The composition of the Earth, *Chem. Geol.*, *120*, 223–253.

McKenzie, D., J. Jackson, and K. Priestley (2005), Thermal structure of oceanic and continental lithosphere, *Earth Planet. Sci. Lett.*, *233*, 337–349.

Mörner, N.-A., and G. Etiope (2002), Carbon degassing from the lithosphere, *Global Planet. Change*, *33*, 185–203.

Muffler, P., and R. Cataldi (1978), Methods for regional assessment of geothermal resources, *Geothermics*, *7*, 53–89.

Müller, R. D., W. R. Roest, J. Y. Royer, L. M. Gahagan, and J. G. Sclater (1997), Digital isochrons of the world's ocean floor, *J. Geophys. Res.*, *102*, 3211–3214.

Pollack, H. N., S. J. Hurter, and J. R. Johnson (1993), Heat-flow from the Earth's interior—Analysis of the global data set, *Rev. Geophys.*, *31*, 267–280.

Ranalli, G. (1987), *Rheology of the Earth*, Allen and Unwin, Boston, Mass.

Rimoldini, L. (2013), Weighted skewness and kurtosis unbiased by sample size, arXiv:1304.6564v2, 1–33.

Rolandone, F., C. Jaupart, J.-C. Mareschal, C. Gariépy, G. Bienfait, C. Carbonne, and R. Lapointe (2003), Surface heat flow, crustal temperatures and mantle heat flow in the Proterozoic Trans-Hudson Orogen, Canadian Shield, *J. Geophys. Res.*, *107*(B12), 2341, doi:10.1029/2001JB000698.

Sass, J. H., A. H. Lachenbruch, and A. M. Jessop (1971), Uniform heat flow in a deep hole in the Canadian Shield and its paleoclimatic implications, *J. Geophys. Res.*, *76*, 8586–8596.

Schmeling, H., and G. Marquart (2013), Coupling hydrothermal convection to a cooling oceanic lithosphere: The effect on the "square root-t" law, *Geophys. Res. Abstr.*, *15*, EGU2013–5558.

Schubert, G., D. Stevenson, and P. Cassen (1980), Whole planet cooling and the radiogenic heat source contents of the Earth and Moon, *J. Geophys. Res.*, *85*, 2531–2538.

Scott, J. R., J. Marotzke, and A. Adcroft (2001), Geothermal heating and its influence on the meridional overturning circulation, *J. Geophys. Res.*, *106*, 31,141–31,154.

Seton, M., et al. (2012), Global continental and ocean basin reconstructions since 200Ma, *Earth Sci. Rev.*, *113*, 212–270.

Shapiro, N. M., and M. H. Ritzwoller (2004), Inferring surface heat flux distributions guided by a global seismic model: Particular application to Antarctica, *Earth Planet. Sci. Lett.*, *223*, 213–224.

Simmons, G., and K. Horai (1968), Heat flow data 2, *J. Geophys. Res.*, *73*, 6608–6609.

Stein, C., and S. Stein (1994), Constraints on hydrothermal flux through the oceanic lithosphere from global heat flow, *J. Geophys. Res.*, *99*, 3081–3095.

Stein, C., and S. Stein (1997), Estimation of lateral hydrothermal flow distance from spatial variations in oceanic heat flow, *Geophys. Res. Lett.*, *24*, 2323–2326.

Talwani, M., X. Le Pichon, and M. Ewing (1965), Crustal structure of the mid-ocean ridges. 2. Computed model from gravity and seismic refraction data, *J. Geophys. Res*, *70*, 341–352.

The KamLAND Collaboration (2011), Partial radiogenic heat model for Earth revealed by geoneutrino measurements, *Nat. Geosci.*, *4*, 647–651.

Theissen-Krah, S., r. K. Iye, L. H. Rüpke, and J. Phipps Morgan (2011), Coupled mechanical and hydrothermal modeling of crustal accretion at intermediate to fast spreading ridges, *Earth Planet. Sci. Lett.*, *311*, 275–286.

Tissot, B. P., R. Pelet, and P. Ungerer (1987), Thermal history of sedimentary basins, maturation indices, and kinetics of oil and gas generation, *AAPG Bull.*, *71*, 1445–1466.

Tsybulya, L. A., and L. S. Sokolova (2002), Heat flow in the region of the Barents and Kara Seas, *Russ. Geol. Geophys.*, *43*, 1049–1052.

Von Herzen, R., E. E. Davis, A. T. Fisher, C. A. Stein, and H. N. Pollack (2005), Comments on "Earth's heat flux revised and linked to chemistry" by A.M. Hoffmeister and R.E. Criss, *Tectonophysics*, *409*, 193–198.

Wei, M., and D. Sandwell (2006), Estimates of heat flow from Cenozoic seafloor using global depth and age data, *Tectonophysics*, *417*, 325–335.